Pergamon

Geochimica et Cosmochimica Acta, Vol. 64, No. 20, pp. 3471–3484, 2000
Copyright © 2000 Elsevier Science Ltd
Printed in the USA. All rights reserved
0016-7037/00 $20.00 + .00

PII S0016-7037(00)00462-2

The depletion and regeneration of dissolution-active sites at the mineral-water interface: I. Fe, Al, and In sesquioxides

SHERRY D. SAMSON,*,† LISA L. STILLINGS,‡ and CARRICK M. EGGLESTON
Department of Geology and Geophysics, University of Wyoming, Laramie, WY 82071-3006 USA

(*Received September* 27, 1999; *accepted in revised form May* 15, 2000)

Abstract—The responses of α-Al_2O_3 and In_2O_3 dissolution rates to pH-jumps in flow-through reactors are compared to previous results for α-Fe_2O_3 in order to test the following hypothesis: because the same fundamental processes of ligand exchange and detachment of metal centers govern both steady state and nonsteady state dissolution, both the steady state and nonsteady state dissolution rates of these sesquioxides correlate with the water exchange rates of the corresponding aqueous ions. Our results show that steady state dissolution rates at pH 1 for α-Fe_2O_3, α-Al_2O_3, and In_2O_3 correlate with the rates of water exchange.

Nonsteady state dissolution rates, in response to jumps to pH 1 from higher initial pH values at which the oxides had been aged, also correlate with water exchange rates although in a complicated way. The amount of solute dissolved during nonsteady state dissolution increases with increasing initial pH, and is consistent with the depletion at low pH and regeneration at higher pH of a reservoir of surface sites active for dissolution at pH 1. This suggests that the oxide surfaces must be sufficiently kinetically dynamic at circumneutral pH for processes to occur that result in the creation of dissolution-active sites. The pH dependence of the amount of solute released can be related to rates of active site production and dissolution, using the idea that hydroxylation of the mineral surface with increasing solution pH has a labilizing effect on the rates of ligand exchange at a surface metal center similar to the labilizing effect of hydrolysis on the rates of water exchange for aquaions. *Copyright © 2000 Elsevier Science Ltd*

1. INTRODUCTION

Mineral dissolution has been the subject of extensive study because of its importance in a variety of geochemical processes ranging from global elemental cycling and climate control to acid rain effects and biochemical strategies for nutrient acquisition. Our understanding of the effects of pH, solution composition, and adsorbed species on dissolution rate is based largely on steady state dissolution measurements. For example, dissolution rates are often related to the concentration of protons or organic (or inorganic) ligands adsorbed to the mineral surface (e.g., Stumm and Wieland, 1990). Such surface complexation approaches to dissolution kinetics are based explicitly on the assumption that the surface is in a steady state configuration; that is, the surface concentration of metal centers participating in dissolution, and their collective overall reactivity toward dissolution, are time independent. Here, in contrast, we utilize pH-jump-induced dissolution transients, caused by temporally changing concentrations and reactivities of dissolution-active surface metal centers, to obtain information about dissolution processes that cannot be obtained from steady state experiments.

Initially elevated dissolution rates that decay to a steady state are a virtually universal observation in mineral dissolution experiments (Holt and King, 1955; Holdren and Berner, 1979; Schott et al., 1981; Chou and Wollast, 1985; Carroll-Webb and Walther, 1988; Knauss et al., 1993; Hellmann, 1995; Maurice et al., 1995; Kraemer and Hering, 1997; Malmström and Banwart, 1997). Occasionally dissolution rates *increase* to a steady state, e.g., quartz at pH > 10 (Knauss and Wolery, 1988). Such initial transients show that the approach of dissolution rate to steady state takes time, and have been attributed to artifacts of sample preparation (Petrovic, 1981a;b; Schott et al., 1981), the formation of altered layers on mineral surfaces (Casey and Bunker, 1990; Hellmann, 1995), or transient adjustments of surface topography or particle size distribution toward a steady state configuration (Holdren and Berner, 1979; Dibble and Tiller, 1981). Rate transients, however, are not limited to the onset of dissolution, but have been reported in response to cycles in pH (Chou and Wollast, 1984; Spokes and Jickells, 1996; Samson and Eggleston, 1998), increases in ligand concentration (Mast and Drever, 1987; Wieland and Stumm, 1992; Kraemer and Hering, 1997), and changes in electrolyte composition (Sjöberg, 1989). Furthermore, such transients have been shown to contain useful information about dissolution mechanisms. For example, Holt and King (1955) related rapid initial dissolution rates to the adsorption of silicic acid to quartz surfaces, and Chou and Wollast (1984) used pH-jump-induced albite dissolution transients to obtain information about the formation, thickness, and composition of altered or leached layers on the feldspar surface. Similarly, we follow these authors in using nonsteady state phenomena as a window on oxide dissolution mechanisms.

A previous study of nonsteady state hematite dissolution (Samson and Eggleston, 1998) showed that following downward pH-jumps to pH 1, a consistent, reproducible, and regenerable nonsteady state period of elevated dissolution rate occurs and lasts for over 36 h. The results were consistent with the

---

*Author to whom correspondence should be addressed (ssamson@deas.harvard.edu).

† *Present address:* Division of Engineering and Applied Sciences, Harvard University, Cambridge, MA 02138 USA.

‡ *Present address:* United States Geological Survey, University of NV-Reno, Reno, NV 89557 USA.

depletion at low pH and regeneration at higher pH of a reservoir of Fe surface sites active for dissolution at pH 1 in response to cycles in pH. Such active sites can be thought of in different ways. We interpreted the data with regard to long-standing crystal growth and dissolution models (e.g., Burton-Cabrera-Frank, BCF; Burton et al., 1951) that assume the existence of "adsorbed nutrient", e.g., Fe^{3+} on hematite, that is structurally distinct from metal centers in the solid surface structure. We attributed the transients to the release of this adsorbed Fe.

Here, we report results for nonsteady state dissolution of corundum (α-Al_2O_3) and cubic indium sesquioxide (In_2O_3) in response to pH-jumps, compare them to results for hematite (α-Fe_2O_3), and use the data to test a simple hypothesis: because the same fundamental processes of ligand exchange and detachment of metal centers govern both steady state and nonsteady state dissolution, both the steady state and nonsteady state dissolution rates of these trivalent metal sesquioxides correlate with the water exchange rates of the corresponding aqueous ions. The model originally developed for hematite (Samson and Eggleston, 1998) is refined in order to describe the wider range of nonsteady state behavior defined by the new data. Finally, we reconsider the idea that the amount of solute released in the transients is directly related to the adsorption of nutrient to the oxide surface (e.g., Fe^{III} to hematite, or Al to corundum), and consider whether the amount of adsorbed nutrient involved in transient dissolution is, at the initial higher pH, controlled by equilibrium or by steady state kinetics.

2. EXPERIMENTAL METHODS

We used the isostructural minerals α-Al_2O_3 and α-Fe_2O_3 (corundum structure, space group $R\bar{3}c$), but a third suitable analog (e.g., corundum structure of a metal with a stable oxidation state and known water exchange rate that differs significantly from those of Al^{3+} and Fe^{3+}) was not readily obtainable. In_2O_3, which has a cubic structure (space group *Ia3*), but the same stoichiometry, was taken as the best alternative.

2.1. Mineral Powders

Hematite was prepared according to a hydrothermal gel-sol method that yields hexagonal platelets 1–2 μm in diameter (Sugimoto et al., 1993). The hematite was suspended in deionized water, centrifuged three times to select particles > 1 μm in diameter, and aged in pH 4.5 solutions (see Samson and Eggleston, 1998, for details). We detected no goethite in XRD or SEM, and a TEM study of hematite made using the same method found no goethite impurity (Shindo et al., 1993).

Corundum was obtained from Sigma-Aldrich as a powder (99% pure and ~100 mesh) and sieved to a 45–75 μm size fraction. The powders were aged in distilled and deionized water for at least one week during which the suspension was centrifuged and decanted at least three times.

The indium oxide was obtained from Sigma-Aldrich as a powder (99.999% pure) and used without further treatment. SEM (JEOL 35CF) revealed a range of particle sizes from sub-micron aggregates of very small particles to single particles up to 10 μm.

Crystal structures were confirmed by powder XRD (Scintag XDS 2000, Cu anode). The specific surface areas for α-Fe_2O_3, α-Al_2O_3, and In_2O_3, as measured with a Quantachrome multipoint N_2 BET instrument, were 4.8, 7.5, and 5.4 $m^2\ g^{-1}$, respectively.

2.2. Analytical Techniques

Total dissolved Fe concentrations were measured by flame atomic absorption, or by the Ferrozine colorimetric method (Stookey, 1970), where greater sensitivity at low concentrations was necessary (≤ 25 ppb). Colorimetric analysis for Fe^{2+} confirmed its absence in the effluent, indicating no significant reductive dissolution had taken place.

Total dissolved Al and In concentrations were determined by ICP-AES or graphite furnace atomic absorption spectroscopy, and ICP-MS, respectively.

2.3. Experimental Conditions

The experiments with In_2O_3 were conducted with the same apparatus used earlier with α-Fe_2O_3 (Samson and Eggleston, 1998): a polycarbonate, water-jacketed, continuous-flow overhead-stirred (~2100 rpm) tank reactor (CSTR). CO_2 was not excluded, and experiments were conducted at 25°C. Cell volume was approximately 95 ml with an In_2O_3 concentration of 7.9 g L^{-1}.

Alumina experiments were conducted with a magnetically-stirred, 75 ml, polycarbonate CSTR (Micro Filtration Systems), modified by adding ports for a pH electrode and acid and base input. To avoid backpressure flow into the electrode, a reservoir of 4M KCl was attached to the electrode and suspended 50 cm above the reactor. Experiments were conducted at ambient laboratory temperature (22 ± 3°C). The α-Al_2O_3 concentration was 25 g L^{-1}

The reactors were pH-statted using HNO_3 (TraceMetal grade, Fisher Scientific) and NaOH (reagent special grade, A.C.S., Spectrum) with software, burettes, and voltmeters from McIntosh Analytical Systems and Ag/AgCl combination electrodes calibrated at pH 2.0, 4.0, and 7.0. Flow rates of ~1 ml min^{-1} for In_2O_3 and α-Fe_2O_3 and ~0.5 ml min^{-1} for α-Al_2O_3 were maintained with peristaltic pumps. The mean residence time of solution within the reactor, $V\ q^{-1}$, where V [L] is the reactor volume and q [L h^{-1}] is the flow rate, was approximately 1.6 h for In_2O_3 and α-Fe_2O_3 and 2.4 h for α-Al_2O_3, giving mixing times (5 residence times; see section 2.4) of approximately 8 h and 12 h, respectively. Effluent was filtered through 0.2 μm cellulose acetate membranes mounted in the base of each CSTR and collected continuously with fraction collectors in acid-washed polypropylene test tubes, 15 min per tube for In_2O_3 and α-Fe_2O_3, and 30 min per tube for α-Al_2O_3.

All solutions were prepared with high purity, 18.2 MΩ-cm water with total organic carbon ≤ 10 ppb (Milli-Q Plus, Millipore). It is important to emphasize that the pH in the reactor and the pH in the input reservoir were changed nearly simultaneously. Specifically, the pump was attached to a new inlet solution reservoir pre-adjusted to the new pH and, at the same time, the pH change in the reactor was made by pipette with concentrated acid (16 N HNO_3) or base (8 N NaOH) in order to accomplish the change as quickly as possible with a minimum increase in volume. Thus, the pH-jump was not limited by the reactor residence time (Eqn. 1), but was effected within seconds (downward pH-jumps) to several minutes (upward pH-jumps).

In two hematite experiments, a series of pH-jumps were imposed in the following sequence of pH: 4.5, 1, 2, 1 for one experiment and 4.5, 1, 3, 1, 2.5, 1, 6, 1 for the other (Samson and Eggleston, 1998). The In_2O_3 experiments consisted of two pH-jumps from pH 4: one to pH 1, and the other to pH 2. Two α-Al_2O_3 experiments utilized the following sequence of pH: 2, l, 5.5, 1 for one experiment and 6.5, 1, 4, 1, 3, 1 for the other.

2.4. Reactor Equations

The response of a well-mixed, continuous-flow reactor to an instantaneous increase in input concentration from zero to $[M]_{in}$, i.e., a step function increase, is an exponential increase in output concentration as a function of volume and flow rate (Perlmutter, 1965):

$$[M]_{out} = [M]_{in}(1 - e^{-t/\tau}) \tag{1}$$

where $[M]_{out}$ [mol L^{-1}] is the dissolved concentration of the metal of interest, M, in the effluent, $[M]_{in}$ [mol L^{-1}] is the dissolved metal concentration in the influent, time t [h] $= 0$ at the time of the step function change in input concentration, and τ [h] is a time constant defining the rate of accumulation of M within the reactor; $\tau = V\ q^{-1}$, the mean residence time of solution within the reactor. Equation 1 assumes constant reactor volume, equal rates of inflow and outflow, and conservative behavior of M (i.e., nonreactive; within the reactor, M is neither produced nor consumed). At $t = 5\tau$, the predicted output

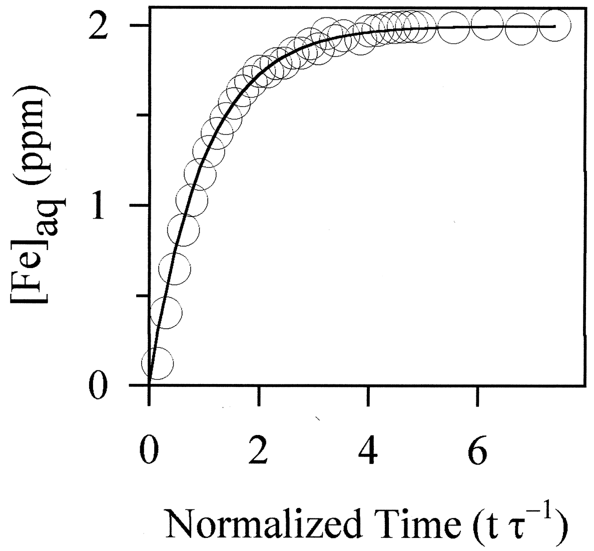

Fig. 1. Outlet Fe concentrations (O) following a change in inlet solution Fe^{3+} concentration from 0 to 2 ppm at $t = 0$. The x-axis is in units of normalized time, $t\,\tau^{-1}$, where τ equals the mean residence time of solution within the reactor ($V\,q^{-1}$). The solid line illustrates the theoretical response predicted by Eqn. 1.

concentration exceeds 99% of the input concentration. Thus, at $t \geq 5\tau$, the new input solution will have displaced the original reactor volume, and the input and output concentrations will be equal, i.e., $[M]_{out} = [M]_{in}$.

An experiment was conducted to determine the degree to which our reactor used in the α-Fe_2O_3 and In_2O_3 experiments approximates an ideal well-mixed reactor. The CSTR initially contained an Fe-free 0.1 N HNO_3 solution and no solid. A 0.1 N HNO_3 input solution containing 2 ppm Fe was fed into the reactor and the Fe output concentration as a function of time was nearly perfectly exponential (Fig. 1) as predicted by Eqn. 1. The suspensions in the dissolution experiments are very dilute (the mineral powders are ~0.15–0.62% by volume), and we therefore assume they are equally well-mixed.

An instantaneous increase in the dissolution rate of a mineral in a CSTR from zero to some constant rate (Fig. 2a) is mathematically equivalent to a step function increase in input concentration (both cases comprise a certain number of moles of *M* input per unit time along with a given volume of input solution per unit time), and the reactor outlet concentration will behave in the same manner (i.e., increase exponentially; Fig. 2b) as described by Eqn. 1.

The interpretation of output that deviates from Eqn. 1 requires an equation for reactor output that separates chemical kinetics from the reactor response. We begin with a nonsteady state material balance equation:

$$V\left(\frac{d[M]_{out}}{dt}\right) = q[M]_{in} - q[M]_{out} + VR_d \tag{2}$$

where $d[M]_{out}/dt$ [mol L^{-1} h^{-1}] is the rate of accumulation of *M* within the reactor, and R_d [mol L^{-1} h^{-1}] is the mineral dissolution rate. The accumulation of dissolved metal within the reactor [mol h^{-1}] is equal to input minus output plus the contribution from dissolution. The initial and boundary conditions are that $q[M]_{in} = 0$ (i.e., there is no detectable Fe, Al, or In in our input solutions), $R_d \cong 0$ at $t < 0$, and at $t > 0$, R_d is constant.

$$\left(\frac{d[M]_{out}}{dt}\right) = R_d - \left(\frac{q}{V}\right)[M]_{out} \tag{3}$$

Solving the differential equation:

$$[M]_{out} = \tau R_d\,(1 - e^{-t/\tau}) \tag{4}$$

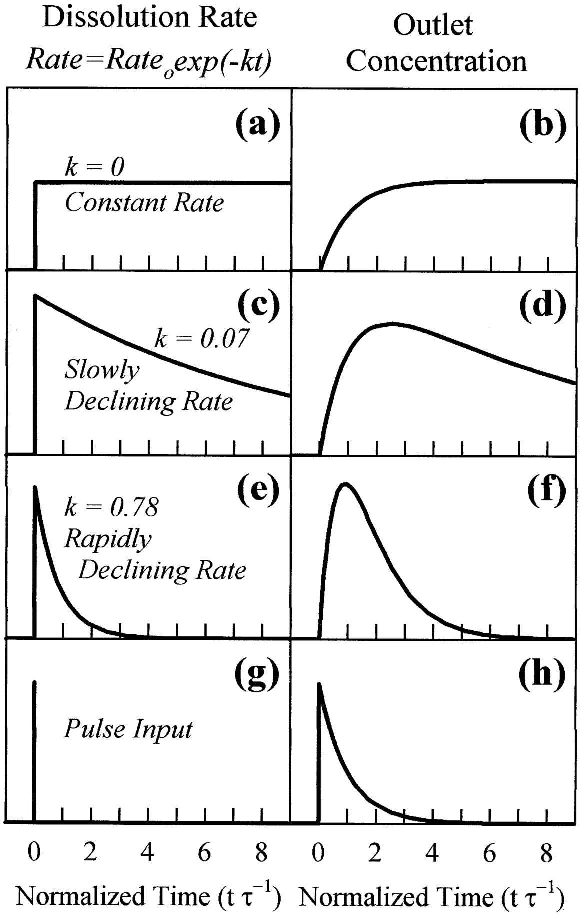

Fig. 2. Outlet concentrations for a mineral in a CSTR in response to an instantaneous increase in dissolution rate at $t = 0$ from zero to $Rate = Rate_o exp(-kt)$: (a,b) constant rate (steady state), (c,d) slowly declining rate, (e,f) rapidly declining rate, and (g,h) pulse input. The values of *k* for which dissolution will be perceived as a pulse input are determined by the reactor residence time and the sampling interval. Units of rate and concentration are omitted.

At infinite time, normalized to surface area, this is the familiar equation for steady state dissolution within a flow-through reactor when $[M]_{in}$ is zero:

$$Rate_{diss} = \left(\frac{q[M]_{out}}{VA}\right) \tag{5}$$

where $Rate_{diss}$ [mol m^{-2} h^{-1}] is the dissolution rate, and *A* [m^2 L^{-1}] is the mineral surface area per unit of solution volume.

For nonsteady state (NSS) dissolution described by a first-order reaction, we replace the constant dissolution rate in Eqn. 3, R_d, with a time-dependent dissolution rate, R_{NSS}:

$$R_{NSS} = R_{NSS_o} e^{-k_1 t} \tag{6}$$

$$\left(\frac{d[M]_{out}}{dt}\right) = R_{NSS_o} e^{-k_1 t} - \left(\frac{q}{V}\right)[M]_{out} \tag{7}$$

where R_{NSS} is in units of mol L^{-1} h^{-1}, R_{NSSo} is R_{NSS} at $t = 0$, and k_1 [h^{-1}] is a decay constant defining an exponential decay in dissolution rate. Solving the differential equation:

$$[M]_{out} = \tau_{NSS} R_{NSS_o} e^{-k_1 t}(1 - e^{-t/\tau_{NSS}}) \tag{8}$$

where the time constant, τ_{NSS}, is now a function of not only volume and

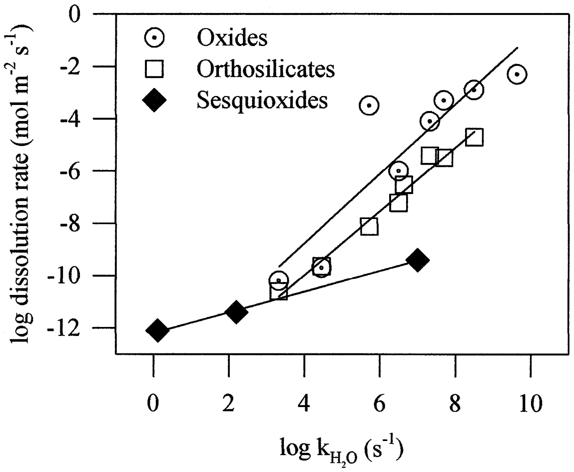

Fig. 3. Steady state dissolution rates in acid solutions for simple divalent oxides (pH 1; Casey, 1991) and nearly-isostructural divalent orthosilicates (pH 2; Casey and Westrich, 1992) and trivalent sesquioxides (pH 1; this study), vs. rate coefficients for the exchange of water molecules between the bulk solution and the inner coordination sphere of the corresponding aqueous cations. Slopes for the oxides, orthosilicates, and sesquioxides are 1.3, 1.2, and 0.4, respectively.

flow rate, but also of the dissolution reaction rate constant: $\tau_{NSS} = V/(q - Vk_1)$.

Figure 2 illustrates the response in outlet concentration corresponding to an instantaneous change in dissolution rate from zero to four types of dissolution rate: steady state (i.e., a constant rate), slowly and rapidly declining rates, and a pulse input (i.e., "instantaneous" dissolution). Fitting the complete range of our data for the different solids required the consideration of all four cases.

3. RESULTS

The steady state dissolution rates at pH 1 for the three sesquioxides correlate with the water exchange rates for the hexaaqua ions (Fig. 3). With respect to nonsteady state dissolution following downward pH-jumps to pH 1, there are consistent, reproducible, pH-dependent transients for all three sesquioxides (Fig. 4) as discussed individually below.

The results of downward pH-jump experiments with hematite (Fig. 4a) are described elsewhere (Samson and Eggleston, 1998). Briefly, following a pH-jump from higher pH to pH 1, the approach to a new steady state dissolution rate takes 36 h or more. The resulting transients are pH-dependent, reproducible, and regenerable.

Here, we present results of hematite upward pH-jumps from pH 1 to pH's 2, 2.5, and 3 (Fig. 5). The fact that Fe is lost from solution more quickly than the reactor time constant would predict indicates rapid sorption or precipitation rather than dilution and washout. The rate of sorption of Fe from solution increases with increasing final pH from pH 2 to pH 3 as indicated in Figure 5 by the time required for Fe concentrations to fall to a new steady state.

Theoretical outlet concentrations that would follow a step function increase in dissolution rate, in response to a downward pH-jump to pH 1, are indicated in Figure 4. Integrating the area between the actual outlet concentrations and the theoretical outlet concentrations gives the amount of Fe (or Al or In) released that can be attributed to nonsteady state chemical kinetics (Fig. 6a). We define this quantity as "excess" Fe, i.e., excess in the sense that it exceeds the steady state reactor outlet concentration at pH 1.

Transient responses resulting from downward pH-jumps to pH 1 with corundum (Fig. 4b) are shorter than for hematite. With the exception of the pH-jump from pH 6.5 to pH 1, they do not extend much beyond the reactor mixing interval (~5τ). Also, except for the pH 2 to pH 1 jump, they start from an initial peak and decay toward a steady state rather than, like hematite, increase to a peak and decline. The amount of excess Al released increases with increasing initial pH, but rather than the gradual increase with increasing pH exhibited by hematite, there is a striking increase in the amount released between initial pH 5.5 and initial pH 6.5 (Fig. 6b).

The downward pH-jumps with In_2O_3 (Fig. 6c) produce transient responses similar to those of hematite, but which resemble the α-Al_2O_3 transients in duration. Rather than pH-jumps to pH 1 from varying initial pH's, there were two pH-jumps from the same initial pH: one from pH 4 to pH 1 and one from pH 4 to pH 2. The steady state dissolution rate is an order of magnitude greater at pH 1 than at pH 2, and the total amount of In released in the interval 0–5τ is also an order of magnitude greater in the jump to pH 1 than in the jump to pH 2.

4. DISCUSSION

Our hypothesis that steady state dissolution rates correlate with the rates of water exchange for the corresponding aqueous ions is supported by the data (Fig. 3). We have also shown that pH-jumps to pH 1 from higher pH consistently produce transients that are initial-pH-dependent, reproducible, and regenerable (Fig. 4).

Because the hematite and corundum powders were cycled between pH 1 and higher pH, the elevated dissolution rates that occur in response to downward pH-jumps might be interpreted as resulting from the dissolution of precipitated (hydr)oxide phases. Metal may precipitate or adsorb from solution during an upward pH-jump from pH 1 (e.g., see Fig. 5) and subsequently re-dissolve upon a return to pH 1. However, using hematite as an example, the amount of Fe in excess of steady state released in 30τ following each pH-jump to pH 1 is a factor of 5 to 26 times greater than that which was available for precipitation or adsorption at the preceding higher pH (Table 1), and therefore this source of Fe alone cannot account for the large amount of Fe released in each transient.

Alternatively, Al_2O_3 surfaces have been observed to transform into hydroxide phases when aged in water, e.g., γ-Al_2O_3 to bayerite following one to four months of aging (Laiti et al., 1998), and α-Al_2O_3 to gibbsite (Liu et al., 1998) or a mixture of gibbsite and bayerite (Lee and Condrate, 1995), both polymorphs of $Al(OH)_3$. The corundum pH-jump from pH 6.5 to pH 1 was preceded by aging of the sample for one week in water, and therefore we cannot rule out a more rapidly soluble surface hydroxide phase as the source of the excess Al released following this downward pH-jump.

In any case, the key result is that the solute released following downward jumps to pH 1 must be derived from the solid itself. If a surface hydroxide phase forms, this transformation probably involves ligand exchange. Likewise, the creation of dissolution-active sites by the step-wise depolymerization of

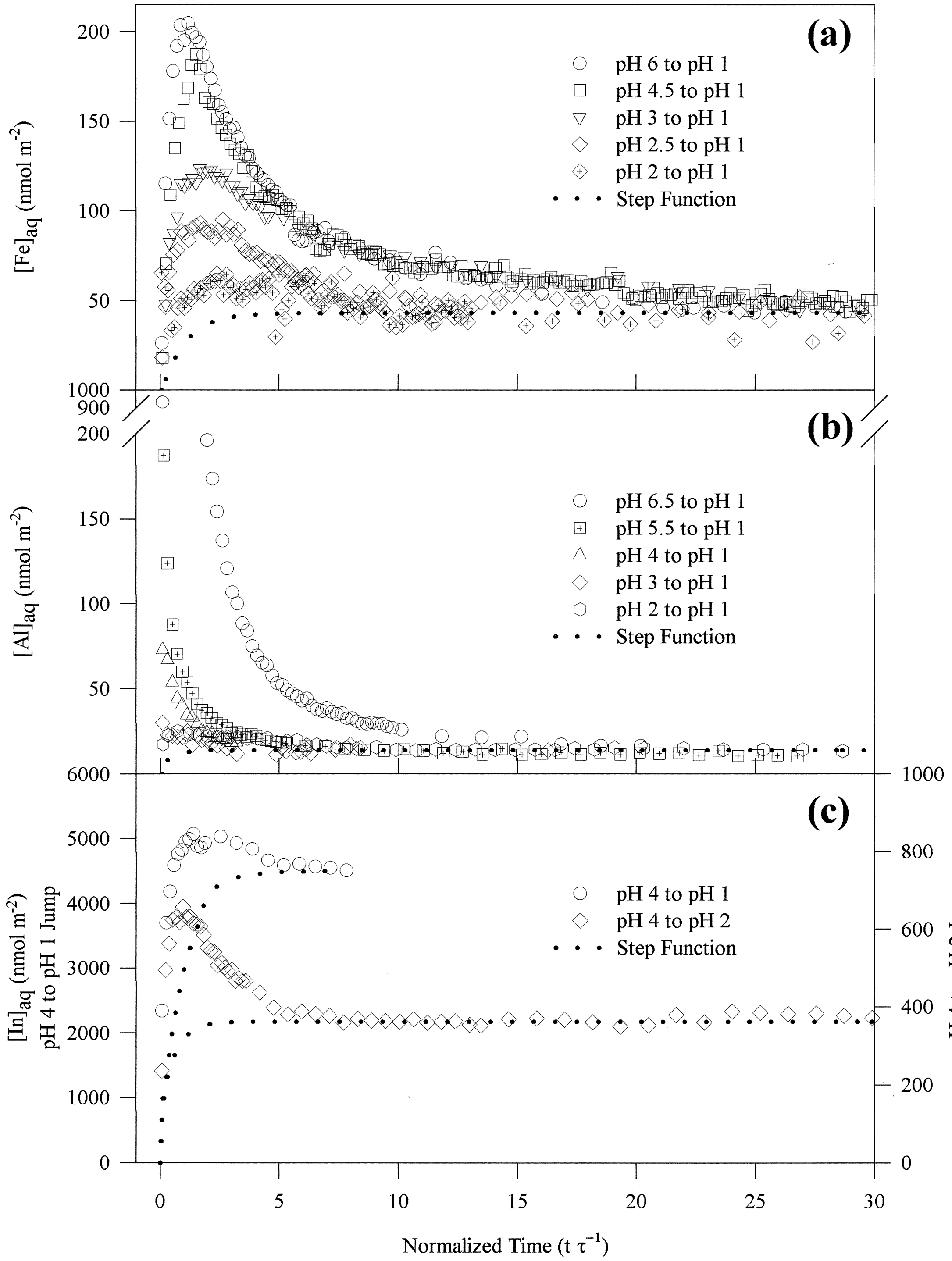

Fig. 4. Results of pH-jump experiments. Time zero represents the time of the pH-jump and pre-jump concentrations were negligible in all cases. Each data series represents the outlet concentrations, normalized to BET surface area, following a jump to pH 1 or 2, as indicated, from the initial pH indicated. Dotted lines illustrate the theoretical response to a step function increase in dissolution rate from zero to a constant steady state rate. (a) α-Fe_2O_3, (b) α-Al_2O_3, and (c) In_2O_3.

lattice metal centers into more labile surface configurations, or by partial dissolution of the solid followed by adsorption of the solute, must also proceed via a ligand exchange process. Therefore, the oxide surfaces must be sufficiently kinetically dynamic at circumneutral pH that processes occur that result in the creation of sites active for dissolution at pH 1.

Previously, we attributed pH-jump-induced dissolution transients for hematite to the release of adsorbed Fe (Samson and

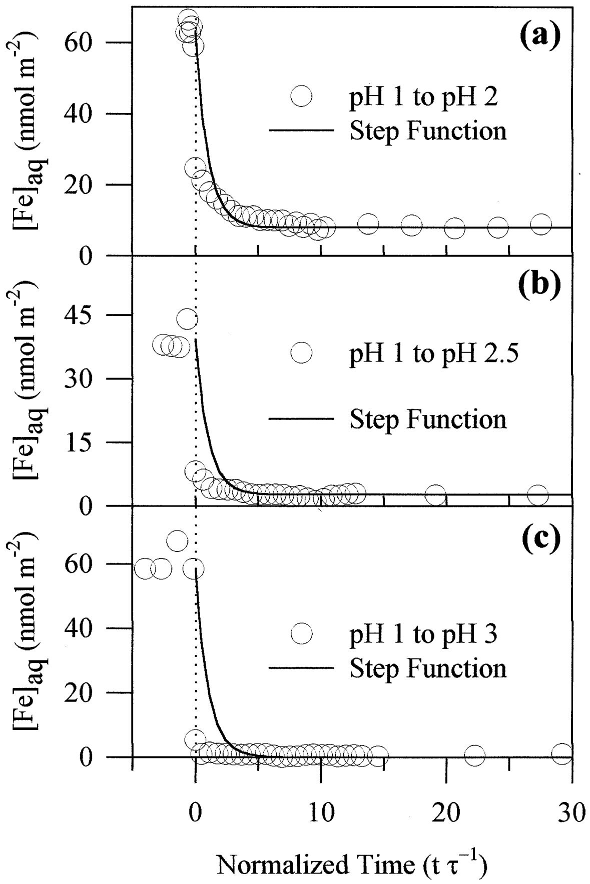

Fig. 5. In response to α-Fe_2O_3 upward pH-jumps at $t = 0$ from pH 1 to (a) pH 2, (b) pH 2.5, and (c) pH 3, the rate of disappearance of Fe from solution increases with increasing final pH. Upward pH-jumps to pH > 3 were not analyzed as Fe concentrations at higher pH are below our analytical detection limits. Solid lines illustrate the theoretical response to a step function decrease in dissolution rate at $t = 0$.

Eggleston, 1998). If the amount of excess metal dissolved in a transient can be described by equilibrium adsorption of nutrient to its oxide, these amounts should be consistent with expected adsorption behavior. The amount of excess Fe released does depend on initial pH in a way similar to the pH-dependence of Fe^{3+} adsorption to other oxides. A plot of excess Fe released vs. initial pH (Fig. 6a) indicates a trend of increasing amounts of excess Fe released with increasing initial pH, and exhibits a break in slope between initial pH's 2.5 and 3. This break in slope is near the first hydrolysis constant for aqueous Fe^{3+}, and is consistent with the value for pH_{50} for Fe^{3+} on α-Al_2O_3 and α-SiO_2 (pH_{50}, the pH at which 50% of the total amount of a solute cation is adsorbed, for Fe^{3+}, on α-Al_2O_3 and α-SiO_2, is between pH 2 and pH 4; Parks, 1990). Consistent with these observations, a Mossbauer study of Fe^{3+} adsorption on hematite (Ambe and Ambe, 1990) reported pH_{60}, i.e., 60% adsorption of Fe^{3+}, at pH 2.5, and our own data show that adsorption of Fe from solution in upward pH-jumps with hematite increases with increasing final pH from pH 2 to pH 3 (Fig. 5). As with hematite, the amount of excess Al released depends on pH in a way similar to the pH-dependence of adsorption of aqueous Al^{3+}. The break in slope near initial pH 5.5 is consistent with the observed value for pH_{50} (approximately pH 5 for Al^{3+} adsorption on amorphous SiO_2; Parks, 1990) and is near the first hydrolysis constant for aqueous Al^{3+}. These observations raise questions that we explore below about the nature and kinetics of processes that generate dissolution-active sites.

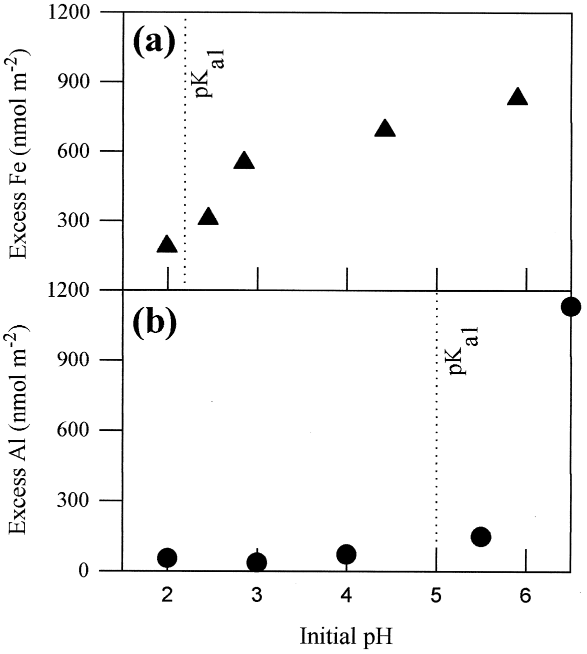

Fig. 6. (a) Excess Fe released in the interval 0–10τ, and (b) excess Al released in the interval 0–5τ, plotted as a function of initial pH. For the α-Al_2O_3 pH 4 to pH 1 pH-jump, the value shown is extrapolated from data for the interval 0–3.1τ. Dotted lines indicate the pH's of the first hydrolysis constants for aqueous (a) Fe^{3+} (2.19; Baes and Mesmer, 1976) and (b) Al^{3+} (5.00; Nordstrom and May, 1996).

4.1. Water Exchange Rates and Dissolution

The length of metal-oxygen bonds in a mineral lattice and the coordination number of the metal center are often similar to those of the hydrated ions in aqueous solution (Casey and Ludwig, 1995). Therefore, as pointed out by Schindler (Casey, 1991), as many as thirty years ago it was suggested that the rates of surface ligand-exchange reactions such as hydration and dissolution might scale in the same manner as the rates of ligand exchange in aqueous solutions (Feitknecht and Hodler,

Table 1. Fe available for adsorption at the time of an upward pH-jump from pH 1 to the pH specified, excess Fe released in 30τ, and the ratio of excess Fe released to Fe available for adsorption.

pH	Fe Available [nmol m^{-2}]	Excess Fe (nmol m^{-2}]	Excess Fe released/Fe available
2	66	347	5.26
2.5	41	387	9.44
3	59	833	14.1
4.5	N/A[a]	948	N/A[a]
6	43	1106	25.7

[a] N/A: Not applicable, 1st pH-jump in the experiment.

1969). Such a relation was not directly shown until more recently (Casey, 1991; Casey and Westrich, 1992; Ludwig et al., 1995; Ludwig et al., 1996). Casey (1991) showed that steady state dissolution rates at pH 1 and pH 2 of a series of simple divalent oxides scale with the water exchange rates for the corresponding aqueous ions (Fig. 3). Casey and Westrich (1992) found a similar correlation for steady state dissolution rates at pH 2 of a series of orthosilicates (Fig. 3), and Westrich et al. (1993) subsequently found that dissolution rates at pH 2 of mixed-cation orthosilicates scale in the same manner as the stoichiometrically-weighted average water exchange rates of the corresponding aqueous cations. The steady state dissolution rates at pH 1 for hematite, corundum, and In_2O_3 (Fig. 3) correlate with the water exchange rates for the hexaaqua ions, but, unlike the divalent oxides and orthosilicates, the slope is clearly far from one, so it cannot be said that the rates *scale* with the water exchange rates.

We discuss the kinetics of water exchange below, but it is not our intent to review the mechanisms of water exchange or the details of coordination chemistry. There is a large body of literature on both the kinetics and mechanisms of water exchange at an aquaion (see Lincoln and Merbach, 1995, for a recent review) and a discussion of this subject as it relates to mineral dissolution may be found in Casey and Ludwig (1995).

To this point, our references to water exchange rates have been confined to the rates of exchange of water molecules between bulk water and the inner coordination sphere of a *fully hydrated* ion, e.g., $Fe(H_2O)_6^{3+}$:

$$Fe(H_2O)_6^{3+} + H_2O^* \leftrightarrow Fe(H_2O)_5(H_2O^*)^{3+} + H_2O \qquad (9)$$

(Margerum et al., 1978). The water exchange rate of an aqueous ion, however, may be enhanced (or inhibited) when one or more coordinated water molecules are replaced by other coordinated species including the hydroxide ion (Margerum et al., 1978; Lincoln and Merbach, 1995). In general, the deprotonation of one of the water molecules in the inner coordination sphere increases the rate of exchange of the remaining water molecules (Margerum et al., 1978). The first deprotonation of $Fe(H_2O)_6^{3+}$ increases the exchange rate of the remaining water molecules by a factor of 750 (Table 2). The labilizing effect of aluminum hydrolysis is even greater: the water exchange rate of $Al(H_2O)_5(OH)^{2+}$ is more than 4 orders of magnitude greater than that of $Al(H_2O)_6^{3+}$ (Table 2).

Although water exchange rates following further hydrolysis, e.g., for the $M(H_2O)_4(OH)_2^+$ species, are not known (and the upper limit for determination of exchange rate coefficients by NMR techniques is about 10^8 s^{-1}; Margerum et al., 1978), support for the premise that sequential deprotonations should further increase the rate of water exchange is found in the observation that the replacement of water molecules by monodentate ligands other than the hydroxide ion can have a progressive labilizing effect on the rate of exchange of the remaining water molecules. Successive substitutions of NH_3 for water molecules in the inner hydration sphere of nickel (II) result in progressive increases in the rate of exchange of the remaining water molecules (Table 2). Similarly, the substitution of F^- ions into the inner coordination sphere of $Al(H_2O)_6^{3+}$ increases the rate of water exchange by a factor of $\sim 10^2$ with each substituting fluoride ion in the monofluoro and difluoro complexes (Table 2). Assuming a progressive effect, Phillips et al. (1997) extrapolated rates for the substitution of three, four, and five fluoride ions.

Table 2. Rate coefficients for the exchange of water molecules from the bulk solution into the inner coordination sphere of hexacoordinated aqueous complexes.

Complex	k_{H_2O} (s^{-1})	Ref.
$Fe(H_2O)_6^{3+}$ (aq)	1.6×10^2	a
$Fe(H_2O)_5(OH)^{2+}$ (aq)	1.2×10^5	a
$Al(H_2O)_6^{3+}$ (aq)	1.3	b
$Al(H_2O)_5(OH)^{2+}$ (aq)	3.1×10^4	c
$AlF(H_2O)_5^{2+}$ (aq)	$1.01\text{–}1.19 \times 10^2$	d
$AlF_2(H_2O)_4^+$ (aq)	1.96×10^4	d
$In(H_2O)_6^{3+}$ (aq)	1.0×10^7	e
$Ni(H_2O)_6^{2+}$ (aq)	2.8×10^4	f
$Ni(H_2O)_5(NH_3)^{2+}$ (aq)	2.5×10^5	g
$Ni(H_2O)_4(NH_3)_2^{2+}$ (aq)	6.1×10^5	g
$Ni(H_2O)_3(NH_3)_3^{2+}$ (aq)	2.5×10^6	g
$Ni(H_2O)(NH_3)_5^{2+}$ (aq)	4.3×10^6	f

[a] (Grant and Jordan, 1981).
[b] (Hugi-Cleary et al., 1985).
[c] (Nordin et al., 1998).
[d] (Phillips et al., 1997).
[e] (Kowall et al., 1998); the value for In^{3+} is a lower limit.
[f] (Jones et al., 1970).
[g] (Desai et al., 1970).

4.2. Surface Ligand Exchange Rates and Active Site Production

If hydroxylation of the oxide surface has a labilizing effect on the ligand exchange rates of metal centers at the mineral surface that is similar to that of hydrolysis for aqueous species, increasing hydroxylation of the surface at circumneutral pH should result in higher ligand exchange rates and, we suggest, more rapid generation of dissolution-active sites, e.g., by depolymerization, than at lower pH where ligand exchange rates are lower. In other words, by analogy with the aqueous ions, qualitatively, the surface metal centers should be more reactive in a ligand exchange sense at neutral pH than at low pH.

Here, we use this idea to examine whether the dependence of the amount of excess solute released in the transients on initial pH can be related to hydrolysis-enhanced rates of ligand exchange, and to explore how the relationship between site generation and site dissolution changes in response to pH-jumps. We use a simplified dissolution reaction to illustrate quantitatively the idea of an interplay between site generation and site dissolution, and to establish the functional form of an equation describing the transition in dissolution rates in response to a pH-jump from circumneutral pH to acidic pH. Although we have related the amount of excess solute dissolved in pH-jump-induced transients to adsorption, we have not shown that adsorption equilibrium has been reached. This section shows how, in the absence of adsorption equilibrium, the pH-dependence of the excess solute can be related to rates of active site production and dissolution. In order to simplify the illustration, back reactions, which increase the complexity of the equations but do not change their functional form, are not presented here.

Consider dissolution as a simplified reaction sequence corresponding to a progression from inactive site (A) to active site

(B) to dissolved species (C), not unlike the concept of a precursor to the activated species (Wieland et al., 1988). We suggest that at circumneutral pH, surface ligand exchange rates are higher than at low pH, and therefore the reaction A → B is fast, but because the concentration of adsorbed protons is limited, the reaction B → C is slow, resulting in a build-up of active sites, B:

$$A \xrightarrow{k_{AB(6)}} B \xrightarrow{k_{BC(6)}} C \tag{10}$$

where $k_{AB(6)}$ and $k_{BC(6)}$ are the net rate constants, e.g., at pH 6, of the forward reactions A → B and B → C, respectively. The rate of change in the concentration of active sites, B, is:

$$\frac{d[B]_6}{dt} = k_{AB(6)}[A] - k_{BC(6)}[B]_6 \tag{11}$$

where *[A]* is the concentration of inactive sites, assumed to be present in excess at all pH's and therefore constant, and $[B]_6$ is the concentration, at pH 6, of B. At steady state, $d[B]_6/dt = 0$, and:

$$[B]_6 = \frac{k_{AB(6)}[A]}{k_{BC(6)}} \tag{12}$$

If $k_{AB(6)}$ is large and $k_{BC(6)}$ is small, the steady state concentration of B will be large.

An identical approach for pH 1 yields a term for the steady state concentration of active sites at pH 1:

$$[B]_1 = \frac{k_{AB(1)}[A]}{k_{BC(1)}} \tag{13}$$

At low pH, we suggest that ligand exchange rates of surface metal centers are slower, and therefore the reaction A → B, inactive site to active site, is slow, but because the concentration of adsorbed protons is high, the reaction B → C, active site to dissolved species, is fast, resulting in a small steady state concentration of active sites, B. Again, we assume inactive sites are present in excess and therefore *[A]* is constant; if $k_{AB(1)}$ is small and $k_{BC(1)}$ is large, the steady state concentration of B will be small.

In response to a pH-jump from higher pH, e.g., pH 6, to pH 1, there will be an initially elevated, but declining, rate of dissolution while the reservoir of active sites, B, is depleted faster than it can be replenished. A new steady state dissolution rate will be reached when the surface site distribution (i.e., the reservoir of active sites, B) is that which is characteristic of steady state at pH 1.

Neglecting the dissolution of any dissolution-active sites which may be generated *during* the transient, the concentration of dissolution-active sites dissolved during the transient is the difference between the steady state concentrations at the initial and final pH's, i.e., $[B]_6 - [B]_1$. Assuming a first-order reaction, the nonsteady state dissolution rate for these sites, $d[C]/dt$, is:

$$\frac{d[C]}{dt} = k_{BC(1)}[B] \tag{14}$$

where *[B]* as a function of time is:

$$[B](t) = ([B]_6 - [B]_1)_o e^{-k_{BC(1)}t} \tag{15}$$

$$[B](t) = \left[\frac{k_{AB(6)}[A]}{k_{BC(6)}} - \frac{k_{AB(1)}[A]}{k_{BC(1)}}\right] e^{-k_{BC(1)}t} \tag{16}$$

An overall equation encompassing both nonsteady state and steady state dissolution includes the rate of dissolution of the excess dissolution-active sites (Eqn.'s 14 and 16) plus the steady state dissolution rate at pH 1:

$$Rate_{diss} = k_{BC(1)}\left[[A]\left(\frac{k_{AB(6)}}{k_{BC(6)}} - \frac{k_{AB(1)}}{k_{BC(1)}}\right)\right] e^{-k_{BC(1)}t} + k_{BC(1)}[B] \tag{17}$$

The exponential term in Eqn. 17 is a function of conditions at both the initial and final pH's, and is represented in our model (section 4.3 below) by exponential terms for the excess dissolution-active sites. Therefore, the concentration of excess dissolution-active sites should be related to initial pH conditions. In our model, as in Eqn. 17, the constant term is the steady state dissolution rate at pH 1.

The term in brackets in Eqn. 17 represents the total concentration of excess dissolution-active surface sites at $t = 0$, $[M_{EX}]_o$. The total amount of excess released in the transients following downward pH-jumps to pH 1 increases with increasing initial pH; to explain these results, the term in brackets must also increase with increasing pH. The terms $k_{AB(1)}$ and $k_{BC(1)}$ will be the same for each of the transients for a given solid for all pH-jumps to pH 1, therefore $[M_{EX}]_o$ can increase only if the ratio $k_{AB(6)}/k_{BC(6)}$ increases with increasing pH. Thus, if equilibrium is not reached during higher pH aging, increasing $[M_{EX}]_o$ must reflect increased values for $k_{AB(6)}/k_{BC(6)}$.

4.3. Model Development

Our original model (Samson and Eggleston, 1998), like Eqn. 17, included only one term for the excess dissolution-active sites and a constant term for steady state dissolution at pH 1. It provided a moderately good fit to the hematite data, but could not fit the corundum data (see Fig. 7).

A minimum of four site types were needed to fit the full range of our data for all three phases: the steady state concentration of sites active for dissolution at pH 1, which are constantly regenerated during dissolution, and three forms of excess dissolution-active sites, which are consumed in a pH-jump from higher pH to pH 1. This does not mean that all site types were needed in all cases, or that there are only four structural types of sites. These are kinetic, not structural, groupings. Conceptually, this simply recognizes that following a downward jump in pH, the more labile of the sites active for dissolution dissolve more quickly, residually enriching the surface in less labile sites, and leading to a temporarily decreasing effective rate coefficient. The four site types represent conceptual groupings of sites with similar rate coefficients and correspond to the four examples in Fig. 2.

The range of extractable rate coefficients is constrained by the reactor residence time and the sampling interval. If the most labile sites dissolve at a rate that is faster than the time resolution of our experimental approach, the dissolution of those sites will be indistinguishable from a pulse input (Fig. 2g,h) and will be perceived as being almost "instantaneous." The remain-

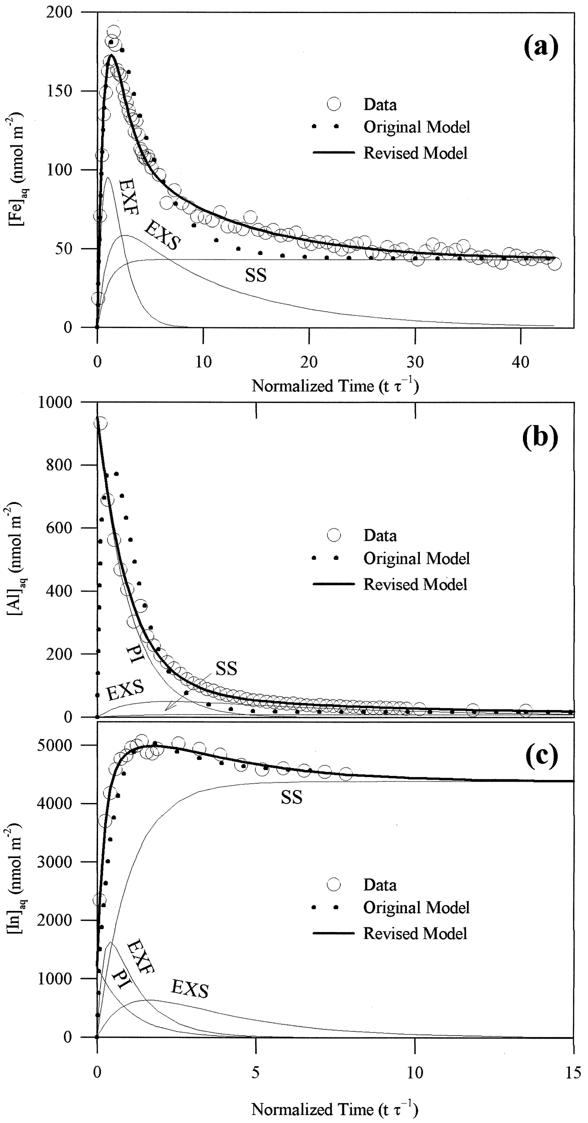

Fig. 7. Representative model fits including curves illustrating the individual parameters comprising the total modeled outlet concentration: steady state (SS), pulse input (PI), fast-dissolving excess (EXF), and slow-dissolving excess (EXS). Also illustrated for comparison are model fits with our original model (dotted lines). (a) α-Fe_2O_3 pH-jump from pH 4.5 to pH 1; (b) α-Al_2O_3 pH-jump from pH 6.5 to pH 1; and (c) In_2O_3 pH-jump from pH 4 to pH 1.

ing excess dissolution-active sites are consumed at rates according to their relative reactivity, one type dissolving rather quickly (Figs. 2e,f) and the other more slowly (Fig. 2c,d).

The overall dissolution rate is assumed to be the sum of the parallel dissolution reactions (assumed to be first-order) taking place at the four types of dissolution-active surface sites:

$$Rate_{diss} = k_{SS1}[>M_{SS1}] + k_{PI}[>M_{PI}] + k_{EXF}[>M_{EXF}] + k_{EXS}[>M_{EXS}] \quad (18)$$

where $[>M_{SS1}]$ [mol m^{-2}] is the constant concentration of surface sites active for dissolution at steady state at pH 1, $[>M_{PI}]$, $[>M_{EXF}]$, and $[>M_{EXS}]$ [mol m^{-2}] are the concentrations of the excess dissolution-active sites (pulse input, fast-dissolving excess, and slowly dissolving excess, respectively), and k_{SS1}, k_{PI}, k_{EXF}, and k_{EXS} [h^{-1}] are the corresponding rate coefficients.

For steady state dissolution in a CSTR in terms of surface concentrations, we rewrite Eqn. 4:

$$[M]_{out} = \tau A Rate_{SS1}(1 - e^{-t/\tau}) \quad (19)$$

where $Rate_{SS1} = k_{SS1}[>M_{SS1}]$ and is in units of mol m^{-2} h^{-1}. We substitute the single term, $Rate_{SS1}$, as it is not possible to extract discrete unique values for k_{SS1} and $[>M_{SS1}]$.

The rate of disappearance of the excess dissolution-active sites is:

$$\frac{-d[>M_{EX}]}{dt} = k_{EX}[>M_{EX}]_o e^{-k_{EX}t} \quad (20)$$

where $[>M_{EX}]$ [mol m^{-2}] represents the concentration at time t, $[>M_{EX}]_o$ [mol m^{-2}] is the initial concentration at $t = 0$, and k_{EX} [h^{-1}] is the rate constant for the consumption of the postulated excess sites. We assume that the rate of disappearance of the excess sites is equal to their dissolution rate, i.e., they are being consumed only by the dissolution process. Consequently, Eqn. 6 and Eqn. 20 are equivalent expressions and:

$$R'_{NSS_o} e^{-k_1 t} = k_{EX}[>M_{EX}]_o e^{-k_{EX}t} \quad (21)$$

where $R'_{NSSo} = R_{NSSo}/A$, the dissolution rate normalized to surface area. Therefore, Eqn. 9 for nonsteady state dissolution in a CSTR, expressed in terms of surface area, is:

$$[M]_{out} = \tau_{EX} A k_{EX}[>M_{EX}]_o e^{-k_{EX}t}(1 - e^{-t/\tau_{EX}}) \quad (22)$$

where $\tau_{EX} = V/(q - Vk_{EX})$.

Equation 22 can be simplified for the sites whose dissolution is perceived as a pulse input. We begin by expanding and rearranging the equation:

$$[M]_{out} = \tau_{PI} A k_{PI}[[>M_{PI}]_o e^{-k_{PI}t} - [>M_{PI}]_o e^{\left(\frac{-qt}{V}\right)}] \quad (23)$$

The magnitude of k_{PI} is large relative to volume (V) and flow rate (q), so

$$\tau_{PI} \cong \frac{1}{-k_{PI}} \quad (24)$$

At $t > 0$, $e^{-k_{PI}t} = 0$, and Eqn. 24 reduces to:

$$[M]_{out} = A[>M_{PI}]_o e^{-t/\tau} \quad (25)$$

The total outlet concentration, $[M]_{TOT}$ [mol L^{-1}], is the sum of the outlet concentrations for the four dissolution reactions (Eqns. 19, 22, and 25):

$$[M]_{TOT} = \tau A Rate_{SS1}(1 - e^{-t/\tau}) + A[>M_{PI}]e^{-t/\tau} + \tau_{EXF} A k_{EXF}[>M_{EXF}]_o e^{-k_{EXF}t}(1 - e^{-t/\tau_{EXF}}) + \tau_{EXS} A k_{EXS}[>M_{EXS}]_o e^{-k_{EXS}t}(1 - e^{-t/\tau_{EXS}}) \quad (26)$$

Table 3. Model parameters (units of $Rate_{SS1}$ are in terms of moles of Fe, Al or In). A value of zero indicates use of the parameter was not required in order to fit the data.

Mineral	α-Fe_2O_3					α-Al_2O_3					In_2O_3	
Initial pH	2	2.5	3	4.5	6	2	3	4	5.5	6.5	4 to 1	4 to 2
K_{EXF} [h^{-1}]	0	0.78	0.78	0.78	0.78	1.78	0	0	0	0	3.38	4.36
K_{EXS} [h^{-1}]	0.07	0.07	0.07	0.07	0.07	0.06	0.06	0	0.06	0.06	0.22	0.46
$[M_{PI}]_o$ [nmol m^{-2}]	43	0	0	0	0	12	29	81	169	953	1217	0
$[M_{EXF}]_o$ [nmol m^{-2}]	0	100	96	249	316	13	0	0	0	0	2424	449
$[M_{EXS}]_o$ [nmol m^{-2}]	217	363	717	772	804	65	34	0	12	475	3249	668
$Rate_{SS1}$ [nmol m^{-2} h^{-1}]	20	26	28	31	25	6	5	6	5	4	2886	216
Total excess [nmol m^{-2}]	260	463	813	1021	1120	90	63	81	181	1428	6890	1117

where $\tau_{EX(F\ or\ S)} = V/(q - Vk_{EX(F\ or\ S)})$. At infinite time, Eqn. 26 reduces to:

$$[M]_{TOT} = \tau A Rate_{SS1} \tag{27}$$

This model differs in two respects from our earlier model (Samson and Eggleston, 1998): the time constant for the excess dissolution-active sites, $\tau_{EX(F\ or\ S)}$, includes the dissolution rate constant, $k_{EX(F\ or\ S)}$, and there are a total of three types of excess dissolution-active sites rather than one. The inclusion of the pulse input parameter allows for the possibility that rate coefficients may be larger than can be resolved given our reactor residence times and sampling intervals, while the use of two parameters for the extractable rate coefficients, rather than one, simply recognizes that the range of rate coefficients for the various excess sites may be sufficiently large that it cannot be adequately represented by only one rate coefficient. Again, we emphasize that these are *kinetic groupings*; we are not suggesting that there are only four structural types of dissolution-active sites.

4.4. Model Fits

Representative model fits are illustrated in Figure 7, and fitted values for the model parameters are shown in Table 3. While this more complex model would be expected to provide a better fit than our earlier model (Samson and Eggleston, 1998) simply by providing more fitting parameters, we point out that fitting for most of the pH-jumps required the use of only two of the three available types of excess dissolution-active sites as indicated by zeros in Table 3. Furthermore, several of these parameters can be independently constrained. The steady state dissolution rate, $Rate_{SS1}$, is fixed by the flow rate and outlet concentration at steady state; the concentration perceived as a pulse input, $[>M_{PI}]$, is constrained by the first outlet concentration following the pH-jump; and, because the relaxation times for hematite extend well beyond the reactor mixing interval of 5τ, the values for k_{EXS} and $[>M_{EXS}]_o$ for hematite may be independently verified as described below.

Following the reactor mixing interval of $\sim 5\tau$, the outlet concentration directly reflects the dissolution rate. Furthermore, solute derived from sites whose dissolution is perceived as a pulse input, $[>M_{PI}]$, will have been washed out of the reactor (see Fig. 2h), and the outlet concentration attributable to steady state dissolution at pH 1 will have reached a constant value (see Fig. 2b). Therefore, by subtracting the steady state outlet concentration from the observed outlet concentrations, we can determine the amount of solute derived from the dissolution of $[>M_{EXF}]$ and $[>M_{EXS}]$ sites. Assuming that the hematite dissolution rate in the interval 5τ to 15τ is dominated by dissolution of the slowly dissolving sites, we can obtain independent values for the parameters k_{EXS} and $[>Fe_{EXS}]_o$ to compare to those obtained from nonlinear least-squares fitting. The values for k_{EXS} and $[>Fe_{EXS}]_o$ are the slope and y-intercept, respectively, of a plot of the natural log of the excess Fe concentration (the measured outlet concentration minus the steady state concentration) vs. time. The average slope of the linear regressions for all data sets was 0.07 (Table 4). With the value for k_{EXS} fixed at 0.07 h^{-1}, the value for k_{EXF} was obtained by optimizing the nonlinear least-squares fit for all data sets. Each of the values for $[>Fe_{EXS}]_o$ obtained by fitting was within 10% of that obtained from the y-intercept of the linear regression (Table 4). The largest contribution to excess Fe dissolution is from the $[>Fe_{EXS}]_o$ term, and a plot of the fitted values for this parameter vs. initial pH (Fig. 8) resembles the observed pattern of actual excess Fe release (Fig. 6a), bolstering our confidence in the multi-site model.

The data for α-Al_2O_3 were modeled with a fixed value of 0.06 h^{-1} for k_{EXS}. The observed pattern of outlet concentration for each of the transients, except the one following the pH 2 to pH 1 jump, is that of a pulse input (Fig. 2h). This means the initial rate coefficient immediately following the pH-jump, k_{PI}, is larger than can be resolved (see section 4.3), and, given the reactor residence time ($\sim$2.4 h) and sampling interval (0.5 h), it must be ≥ 7 h^{-1}. The largest contribution to the excess Al dissolution rate is from the $[>Al_{PI}]$ term (Table 3).

The data for In_2O_3 for the pH 4 to pH 1 pH-jump were modeled with a value of 0.22 h^{-1} for k_{EXS}. As with hematite, the largest contribution to excess dissolution is from the slowly

Table 4. α-Fe_2O_3 model parameter comparison. The values for k_{EXS} and $[>Fe_{EXS}]_o$, Linear Regression, are from linear regressions of the data (see section 4.4 for details). The values for $[>Fe_{EXS}]_o$, Fitting, are from nonlinear least-squares fitting with k_{EXS} and k_{EXF} fixed at 0.07 h^{-1} and 0.78 h^{-1}, respectively.

		$[>Fe_{EXS}]_o$ (nmol m^{-2})	
Initial pH	k_{EXS} (h^{-1})	Linear Regression	Fitting
2	0.08	218	217
2.5	0.08	329	363
3	0.06	752	717
4.5	0.07	730	772
6	0.07	846	804

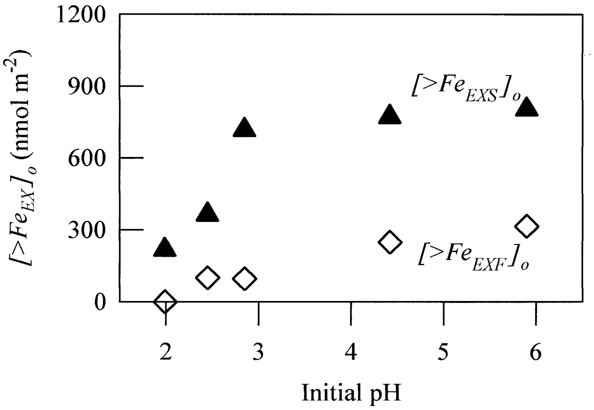

Fig. 8. α-Fe_2O_3 fitted model parameters $[>Fe_{EXF}]_o$ and $[>Fe_{EXS}]_o$ plotted as a function of initial pH.

dissolving excess sites, the $[>In_{EXS}]_o$ term, but the relatively high steady state dissolution rate dominates the overall dissolution rate (Table 3).

In summary, the rate coefficient for the slowly declining dissolution rate approaching a new steady state, i.e., the "tail" of the transient, increases with the water exchange rate (Fig. 9a). A comparison of rate coefficients for the more rapid initial dissolution is, of necessity, more qualitative than quantitative because some rate coefficients are larger than can be resolved. Despite the uncertainties, however, it appears that the trend in the rapid initial dissolution rates resembles the trend in the hydrolysis constants of the aqueous ions (Fig. 9b), reflecting the influence of conditions at the initial pH on dissolution rates immediately following the pH-jump as predicted by Eqn. 17.

We have made a case for ligand exchange rates of surface metal centers that are faster in the circumneutral pH region than at low pH, and our experimental observations strongly suggest that dissolution-active sites are generated most rapidly at circumneutral pH, whereas overall oxide dissolution rates decrease as one goes from the acid to circumneutral pH region. A resolution of this apparent contradiction was suggested by the discussion in section 4.2 in which the creation of dissolution-active sites and detachment are considered to be consecutive reactions with the net rate of dissolution controlled by the slowest step. In the illustration, proton adsorption kinetics are rate-limiting at circumneutral pH and surface ligand exchange rates are rate-limiting at low pH. We now use this idea to examine the steady state dissolution rates observed at low pH.

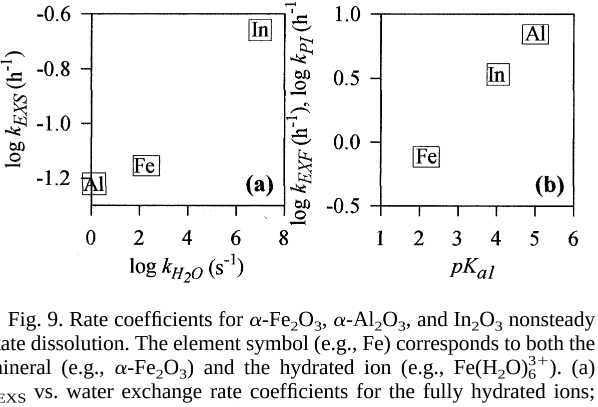

Fig. 9. Rate coefficients for α-Fe_2O_3, α-Al_2O_3, and In_2O_3 nonsteady state dissolution. The element symbol (e.g., Fe) corresponds to both the mineral (e.g., α-Fe_2O_3) and the hydrated ion (e.g., $Fe(H_2O)_6^{3+}$). (a) k_{EXS} vs. water exchange rate coefficients for the fully hydrated ions; and (b) k_{EXF} or k_{PI} vs. the first hydrolysis constants for the aqueous ions. With respect to (b), the values for Fe and In are the fitted values for k_{EXF} (see Table 3); k_{PI} for Al is not known and the value shown is a lower limit (see section 4.2). The value for In is also a lower limit since the pH 4 to pH 1 pH-jump includes rate coefficient k_{PI} in addition to k_{EXF}.

4.5. The Interplay of Ligand Exchange Rates and Surface Protonation

A surface complexation rate law for steady state proton-promoted dissolution, in the absence of specifically adsorbing ligands, can be expressed as:

$$Rate_H = k_H\,(C_H)^n \tag{28}$$

where the dissolution rate, $Rate_H$, is in units of mol m^{-2} h^{-1}, k_H [h^{-1}] is a rate constant for proton-promoted dissolution, (C_H) [mol m^{-2}] is the concentration of adsorbed protons in excess relative to the point of zero proton charge, and n is an empirical rate order (Furrer and Stumm, 1986). C_H, and thus dissolution rate, increases with decreasing solution pH, and the model predicts that once a point of maximum proton adsorption is reached, the steady state dissolution rate will become independent of pH. Observations of dissolution rates that appear to be constant below a given pH have been interpreted as evidence of saturation of the oxide surface with adsorbed protons (Furrer and Stumm, 1986; Wieland et al., 1988). Casey et al. (1993) found the dissolution rates of α-Al_2O_3 at pH 1 and pH 2 to be nearly identical ($10^{-13.1}$–$10^{-12.7}$ and $10^{-12.8}$ mol m^{-2} s^{-1}, respectively). Carroll-Webb and Walther (1988) also observed nearly constant dissolution rates for corundum at pH $\leq$ 3 ($\sim 10^{-12.7}$ mol m^{-2} s^{-1}), similar to the pH-independence of the dissolution rates of δ-Al_2O_3 below pH 3.5 observed by Furrer and Stumm (1986). If this plateau in the dissolution rates of Al_2O_3 at low pH is due to saturation of the surface with adsorbed protons, one might expect the dissolution behavior of hematite to resemble that of corundum since the two phases are isostructural, have similar points of zero charge (pH_{pzc} is 8.9 for corundum and 8.5 for hematite; Sahai and Sverjensky, 1997), and their proton adsorption isotherms are nearly the same when plotted as a function of ΔpH ($\Delta pH = pH_{pzc} - pH$; Wieland et al., 1988). However, the hematite steady state dissolution rate is an order of magnitude greater at pH 1 than at pH 2 ($10^{-11.4}$–10^{-11} and $10^{-12.3}$ mol m^{-2} s^{-1}, respectively; this study). We suggest that the difference in the dissolution rate behavior for corundum and hematite at low pH is due to the difference in their ligand exchange rates.

The weighted average rate coefficient, $k_{H_2O,avg}$, for water exchange for the aqueous ions M^{3+} and MOH^{2+} is:

$$k_{H_2O,avg} = \frac{k_{H_2O,M^{3+}}[M^{3+}] + k_{H_2O,MOH^{2+}}[MOH^{2+}]}{[M^{3+}] + [MOH^{2+}]} \tag{29}$$

At pH 2, $k_{H_2O,avg}$ values for Fe^{III} and Al are 4.7×10^4 s^{-1} and 3.2×10^1 s^{-1}, respectively. The water exchange rate for $InOH(H_2O)_5^{2+}$ is not known, but the lower limit of $k_{H_2O,M^{3+}}$ for In^{3+} is 1.0×10^7 s^{-1} (Kowall et al., 1998), and, like hematite, the steady state dissolution rate of In_2O_3 is nearly an order of magnitude greater at pH 1 than at pH 2 ($10^{-9.4}$ and $10^{-10.5}$ mol m^{-2} s^{-1}, respectively; this study), in close agreement with the earlier findings of Casey et al. (1993) ($10^{-9.5}$ and $10^{-10.25}$ mol m^{-2} s^{-1}, respectively). Using aqueous water exchange rates as a proxy for surface ligand exchange rates, the comparatively slow ligand exchange rate for Al suggests that surface ligand exchange may be the rate-limiting step for corundum dissolution below pH 3. In contrast, because the steady state dissolution rates for both hematite and In_2O_3 increase by approximately one order of magnitude with an order of magnitude increase in the H^+ ion activity from pH 2 to pH 1, proton adsorption kinetics appear to be rate limiting for these solids at pH $\geq$ 1. The fact that these increases in dissolution rate with decreasing pH occur in a pH region where one might expect the surface to be saturated with adsorbed protons suggests that solution pH may affect dissolution rate even after a condition of maximum proton adsorption has been achieved.

5. CONCLUSIONS AND SUMMARY

1. The steady state dissolution rates of α-Fe_2O_3, α-Al_2O_3, and In_2O_3 at pH 1 correlate with the water exchange rates of the corresponding aqueous ions. The range in the dissolution rates for the three phases, however, is considerably less than the 7 orders of magnitude difference in the water exchange rates for the aqueous ions, suggesting that factors other than the inherent properties of the metal may limit the extent to which dissolution rates vary for isostructural (or nearly isostructural) minerals.
2. The very rapid dissolution rates immediately following a downward pH-jump to pH 1 do not correlate with the water exchange rates. They, however, do correlate with the first hydrolysis constants for the aqueous ions, reflecting the influence of conditions at the initial pH on dissolution rates immediately following the pH-jump. The amount of solute dissolved increases with increasing initial pH consistent with either:

    - an equilibrium concentration of adsorbed nutrient as a function of initial pH; or
    - the idea that hydroxylation of the mineral surface with increasing solution pH has a labilizing effect on the rates of ligand exchange at a surface metal center similar to the labilizing effect of hydrolysis on the rates of water exchange for aquaions.

    The next paper in this series (Samson and Eggleston, 2000) explores the rate at which dissolution-active sites are created, allowing us to address the question of whether or not equilibrium with regard to nutrient adsorption was closely approached at the initial pH's studied here.

3. The rates for nonsteady state dissolution of α-Fe_2O_3, α-Al_2O_3, and In_2O_3 in response to downward pH-jumps to pH 1, approaching a new steady state, correlate weakly with the water exchange rates of the corresponding aqueous ions. This suggests that, following an initial period of very rapid dissolution, the rate of approach to a new steady state is a function of the rate at which the reservoir of active sites is replenished at pH 1, i.e., the rate of ligand exchange at pH 1.
4. The pH-independence of Al_2O_3 dissolution rates at pH $\leq$ 3 may be an indication that surface ligand exchange is the rate-limiting step in alumina dissolution at low pH.
5. The pH-dependence of α-Fe_2O_3 and In_2O_3 dissolution rates at pH 1 and pH 2 suggests that rates of proton adsorption continue to be relevant at low pH, even when the mineral surface may be saturated with adsorbed protons, and may be the rate-limiting step in the dissolution of metals with relatively high ligand exchange rates.

The wide range of potential coordinative environments for metal centers at a mineral surface suggests that the range of ligand exchange rates for surface metals will likely be much greater than those of aqueous monomers. Nonetheless, the parallels between trends in ligand exchange rates for aqueous species and the observed patterns in the depletion and regeneration of dissolution-active sites at the mineral-water interface are intriguing, and suggest that trends in ligand exchange rates for aqueous species may be useful as an indication of the relative reactivity, in a ligand exchange sense, of lattice metal centers. If the relationships between ligand exchange and proton adsorption that we have suggested can be shown to be consistent with the nonsteady state dissolution behavior of other nearly isostructural oxides and silicates, not only will they be important for understanding nonsteady state kinetics, but they can provide insights into the processes that control steady state dissolution rates.

Acknowledgments—We are grateful to Pradeep Agarwal and Steve Higgins for their valuable assistance with the reactor equations. We also thank Steve Boese for analytical assistance, and three anonymous reviewers for their thorough reviews and helpful comments. Financial support was provided by The National Science Foundation (Grant #EAR-9527031 to CME).

REFERENCES

Ambe S. and Ambe F. (1990) Mossbauer study of ferric ions adsorbed at α-ferric oxide/aqueous solution interface. *Langmuir* **6,** 644–649.

Baes C. F., Jr. and Mesmer R. E. (1976) The Hydrolysis of Cations. John Wiley & Sons, Inc.

Burton W. K., Cabrera N., and Frank F. C. (1951) The growth of crystals and the equilibrium structure of their surfaces. *Phil. Trans. Roy. Soc. London Ser. A.* **243(A.866),** 299–358.

Carroll-Webb S. A. and Walther J. V. (1988) A surface complex reaction model for the pH-dependence of corundum and kaolinite dissolution rates. *Geochim. Cosmochim. Acta* **52,** 2609–2623.

Casey W. H. (1991) On the relative dissolution rates of some oxide and orthosilicate minerals. *J. Colloid Interface Sci.* **146(2),** 586–589.

Casey W. H., Banfield J. F., Westrich H. R., and McLaughlin L. (1993) What do dissolution experiments tell us about natural weathering? *Chem. Geol.* **105,** 1–15.

Casey W. H. and Bunker B. (1990) Leaching of mineral and glass surfaces during dissolution. In *Mineral-Water Interface Geochemistry* (ed. M. F. Hochella, Jr. and A. F. White), Vol. 23, pp. 397–426. Mineralogical Society of America.

Casey W. H. and Ludwig C. (1995) Silicate mineral dissolution as a ligand-exchange reaction. In *Chemical Weathering Rates of Silicate Minerals* (ed. A. F. White and S. L. Brantley), Vol. 31, pp. 87–117. Mineralogical Society of America.

Casey W. H. and Westrich H. R. (1992) Control of dissolution rates of orthosilicate minerals by divalent metal-oxygen bonds. *Nature* **355,** 157–159.

Chou L. and Wollast R. (1984) Study of the weathering of albite at room temperature and pressure with a fluidized bed reactor. *Geochim. Cosmochim. Acta* **48,** 2205–2217.

Chou L. and Wollast R. (1985) Steady-state kinetics and dissolution mechanisms of albite. *Am. J. Sci.* **285,** 963–993.

Desai A. G., Dodgen H. W., and Hunt J. P. (1970) Water exchange between solvent and aquoamminenickel (II) complexes. *J. Am. Chem. Soc.* **92(4),** 798–801.

Dibble W. E., Jr. and Tiller W. A. (1981) Non-equilibrium water/rock interactions-I. Model for interface-controlled reactions. *Geochim. Cosmochim. Acta* **45,** 79–92.

Feitknecht W. and Hodler M. (1969) Über die hydratation von nickeloxid. *Z. Phys. Chem. N. F.* **64,** 141–144.

Furrer G. and Stumm W. (1986) The coordination chemistry of weathering: I. Dissolution kinetics of δ-Al_2O_3 and BeO. *Geochim. Cosmochim. Acta* **50,** 1847–1860.

Grant M. and Jordan R. B. (1981) Kinetics of solvent water exchange on iron (III). *Inorg. Chem.* **20,** 55–60.

Hellmann R. (1995) The albite-water system: Part II. The time-evolution of the stoichiometry of dissolution as a function of pH at 100, 200, and 300°C. *Geochim. Cosmochim. Acta* **59(9),** 1669–1697.

Holdren G. R., Jr. and Berner R. A. (1979) Mechanism of feldspar weathering-I. Experimental studies. *Geochim. Cosmochim. Acta* **43,** 1161–1171.

Holt P. F. and King D. T. (1955) The chemistry of silica surfaces. *J. Chem. Soc. London*, Part I: 773–779.

Hugi-Cleary D., Helm L., and Merbach A. E. (1985) Variable-temperature and variable-pressure ^{17}O-NMR study of water exchange of hexaaquaaluminium(III). *Helv. Chim. Acta* **68,** 545–554.

Jones J. P., Billo E. J., and Margerum D. W. (1970) The effect of coordinated ligands on the rate of replacement of bound water by ammonia in nickel (II) complexes. *J. Amer. Chem. Soc.* **92(7),** 1875–1880.

Knauss K. G., Nguyen S. N., and Weed H. C. (1993) Diopside dissolution kinetics as a function of pH, CO_2, temperature, and time. *Geochim. Cosmochim. Acta* **57,** 285–294.

Knauss K. G. and Wolery T. J. (1988) The dissolution kinetics of quartz as a function of pH and time at 70°C. *Geochim. Cosmochim. Acta* **52(1),** 43–53.

Kowall T., Caravan P., Bourgeois H., Helm L., Rotzinger F. P., and Merbach A. E. (1998) Interpretation of activation volumes for water exchange reactions revisited: *Ab initio* calculations for Al^{3+}, Ga^{3+}, and In^{3+}, and new experimental data. *J. Amer. Chem. Soc.* **120,** 6569–6577.

Kraemer S. M. and Hering J. G. (1997) Influence of solution saturation state on the kinetics of ligand-controlled dissolution of oxide phases. *Geochim. Cosmochim. Acta* **61**(14), 2855–2866.

Laiti E., Persson P., and Öhman L.-O. (1998) Balance between surface complexation and surface phase transformation at the alumina/water interface. *Langmuir* **14,** 825–831.

Lee D. H. and Condrate R. A., Sr. (1995) An FTIR spectral investigation of the structural species found on alumina surfaces. *Mater. Lett.* **23,** 241–246.

Lincoln S. F. and Merbach A. E. (1995) Substitution reactions of solvated metal ions. In *Advances in Inorganic Chemistry* (ed. A. G. Sykes), Vol. 42, pp. 1–88. Academic Press, Inc.

Liu P., Kendelewicz T., Brown G. E., Jr., Nelson E. J., and Chambers S. A. (1998) Reaction of water vapor with α-Al_2O_3 (0001) and α-Fe_2O_3 (0001) surfaces: Synchrotron X-ray photoemission studies and thermodynamic calculations. *Surface Sci.* **417,** 53–65.

Ludwig C., Casey W. H., and Rock P. A. (1995) Prediction of ligand-promoted dissolution rates from the reactivities of aqueous complexes. *Nature* **375,** 44–47.

Ludwig C., Devidal J.-L., and Casey W. H. (1996) The effect of different functional groups on the ligand-promoted dissolution of NiO and other oxide minerals. *Geochim. Cosmochim. Acta* **60(2),** 213–224.

Malmström M. and Banwart S. (1997) Biotite dissolution at 25°C: The pH dependence of dissolution rate and stoichoimetry. *Geochim. Cosmochim. Acta* **61(14),** 2779–2799.

Margerum D. W., Cayley G. R., Weatherburn D. C., and Pagenkopf G. K. (1978) Kinetics and mechanisms of complex formation and ligand exchange. In *Coordination Chemistry, Volume 2* (ed. A. E. Martell), Vol. 174, pp. 1–220. American Chemical Society.

Mast M. A. and Drever J. I. (1987) The effect of oxalate on the dissolution rates of oligoclase and tremolite. *Geochim. Cosmochim. Acta* **51,** 2559–2568.

Maurice P. A., Hochella M. F., Jr., Parks G. A., Sposito G., and Schwertmann U. (1995) Evolution of hematite surface microtopography upon dissolution by simple organic acids. *Clays Clay Mineral.* **43(1),** 29–38.

Nordin J. P., Sullivan D. J., Phillips B. L., and Casey W. H. (1998) An ^{17}O-NMR study of the exchange of water on $AlOH(H_2O)_5^{2+}$(aq). *Inorg. Chem.* **37,** 4760–4763.

Nordstrom D. K. and May H. M. (1996) Aqueous equilibrium data for mononuclear aluminum species. In *The Environmental Chemistry of Aluminum* (ed. G. Sposito), pp. 39–80. CRC Press, Inc.

Parks G. A. (1990) Surface energy and adsorption at mineral-water interfaces: An introduction. In *Mineral-Water Interface Geochemistry* (ed. M. F. Hochella, Jr. and A. F. White), Vol. 23, pp. 133–175. Mineralogical Society of America.

Perlmutter D. D. (1965) Introduction to Chemical Process Control. John Wiley & Sons, Inc.

Petrovic R. (1981a) Kinetics of dissolution of mechanically comminuted rock-forming oxides and silicates. I. Deformation and dissolution of quartz under laboratory conditions. *Geochim. Cosmochim. Acta* **45,** 1665–1674.

Petrovic R. (1981b) Kinetics of dissolution of mechanically comminuted rock-forming oxides and silicates. II. Deformation and dissolution of oxides and silicates in the laboratory and at the earth's surface. *Geochim. Cosmochim. Acta* **45,** 1675–1686.

Phillips B. L., Casey W. H., and Crawford S. N. (1997) Solvent exchange in $AlF_x(H_2O)_{6-x}^{3-x}$(aq) complexes: Ligand-directed labilization of water as an analogue for ligand-induced dissolution of oxide minerals. *Geochim. Cosmochim. Acta* **61(15),** 3041–3049.

Sahai N. and Sverjensky D. A. (1997) Evaluation of internally consistent parameters for the triple-layer model by the systematic analysis of oxide surface titration data. *Geochim. Cosmochim. Acta* **61(14),** 2801–2826.

Samson S. D. and Eggleston C. M. (1998) Active sites and the non-steady-state dissolution of hematite. *Env. Sci. Techl.* **32,** 2871–2875.

Samson S. D. and Eggleston C. M. (2000) The depletion and regeneration of dissolution-active sites at the mineral-water interface: II. α-Fe_2O_3 at pH 3 and pH 6. *Geochim. Cosmochim. Acta* This issue.

Schott J., Berner R. A., and Sjöberg E. L. (1981) Mechanism of pyroxene and amphibole weathering: I. Experimental studies of iron-free minerals. *Geochim. Cosmochim. Acta* **45,** 2123–2135.

Shindo D., Lee B.-T., Waseda Y., Muramatsu A., and Sugimoto T. (1993) Crystallography of platelet-type hematite particles by electron microscopy. *Mater. Trans. JIM* **34(7),** 580–585.

Sjöberg L. (1989) Kinetics and non-stoichiometry of labradorite dissolution. In *Water-Rock Interaction WRI-6* (ed. D. L. Miles), pp. 639–642. A. A. Belkema.

Spokes L. J. and Jickells T. D. (1996) Factors controlling the solubility of aerosol trace metals in the atmosphere and on mixing into seawater. *Aquatic Geochem.* **1,** 355–374.

Stookey L. L. (1970) Ferrozine—a new spectrophotometric reagent for iron. *Anal. Chem.* **42(7),** 779–781.

Stumm W. and Wieland E. (1990) Dissolution of oxide and silicate minerals: Rates depend on surface speciation. In *Aquatic Chemical Kinetics: Reaction Rates of Processes in Natural Waters* (ed. W. Stumm), pp. 367–400. John Wiley & Sons, Inc.

Sugimoto T., Muramatsu A., Sakata K., and Shindo D. (1993) Characterization of hematite particles of different shapes. *J. Colloid Interface Sci.* **158,** 420–428.

Westrich H. R., Cygan R. T., Casey W. H., Zemitis C., and Arnold G. W. (1993) The dissolution kinetics of mixed-cation orthosilicate minerals. *Am. J. Sci.* **293,** 869–893.

Wieland E. and Stumm W. (1992) Dissolution kinetics of kaolinite in acidic aqueous solutions at 25°C. *Geochim. Cosmochim. Acta* **56,** 3339–3357.

Wieland E., Wehrli B., and Stumm W. (1988) The coordination chemistry of weathering: III. A generalization on the dissolution rates of minerals. *Geochim. Cosmochim. Acta* **52,** 1969–1981.

APPENDIX: LIST OF SYMBOLS

$>$:	denotes bonds to the mineral surface
A [m^{2} L^{-1}]:	mineral surface area per unit of reactor volume
(C_H) [mol m^{-2}]:	concentration of adsorbed protons in excess relative to the point of zero proton charge (Eqn. 28)
$d[M]_{out}/dt$ [mol L^{-1} h^{-1}]:	rate of accumulation of the dissolved metal of interest, M, within the reactor
k [h^{-1}]:	dissolution rate constant (steady state dissolution) or coefficient (nonsteady state dissolution); subscripts denote specific site types
k_{EX}:	all excess dissolution-active sites
k_{EXF}:	fast-dissolving excess sites
k_{EXS}:	slow-dissolving excess sites
k_H:	proton-promoted dissolution (Eqn. 28)
k_{PI}:	excess sites whose dissolution is perceived as a pulse input
k_{SS1}:	the constant concentration of surface sites active for dissolution at steady state at pH 1
k_1 [h^{-1}]:	decay constant defining an exponential decay in dissolution rate
k_{H_2O} [s^{-1}]:	rate of exchange of water molecules between bulk water and the inner coordination sphere of a hydrated complex, e.g., $Fe(H_2O)_6^{3+}$
$k_{H_2O,avg}$ [s^{-1}]:	apparent water exchange rate coefficient; the weighted average of the water exchange rates of a hydrated cation and its hydrolysis products
M:	solute of interest, e.g., Fe, Al, or In
$[M]_{in}$, $[M]_{out}$ [mol L^{-1}]:	dissolved concentration of M in the reactor influent and effluent, respectively
$[M]_{TOT}$ [mol L^{-1}]:	total dissolved concentration of M in the reactor effluent as defined by Eqn. 26
$[>M_{EX}]$ [mol m^{-2}]:	total concentration, at time t, of all excess dissolution-active surface sites which are consumed in a pH-jump from higher pH to pH 1; subscripts denote specific site types; the initial concentration at $t = 0$ is denoted as follows: $[>M_{EX}]_o$
$[>M_{EXF}]$:	fast-dissolving excess sites
$[>M_{EXS}]$:	slow-dissolving excess sites
$[>M_{PI}]$:	sites whose dissolution is perceived as a pulse input
$[>M_{SS1}]$ [mol m^{-2}]:	constant concentration of surface sites active for dissolution at steady state at pH 1
n:	an empirical rate order, ideally corresponding to the number of protonation steps prior to detachment of the metal center (Eqn. 28)
pH_{50}:	the pH at which 50% of the total amount of a solute cation is adsorbed
pH_{pzc}:	the pH of zero proton charge
pK_{a1}:	negative log of the equilibrium constant for the first hydrolysis reaction for an aqueous cation
q [L h^{-1}]:	flow rate
R_d [mol L^{-1} h^{-1}]:	mineral dissolution rate; a constant (Eqn. 2)
R_{NSS} [mol L^{-1} h^{-1}]:	time-dependent dissolution rate for nonsteady state dissolution; first-order reaction
R_{NSSo} [mol L^{-1} h^{-1}]:	R_{NSS} at $t = 0$
R'_{NSSo} [mol m^{-2} h^{-1}]:	R_{NSSo} normalized to BET surface area; equals R_{NSSo}/A
$Rate_{diss}$ [mol m^{-2} h^{-1}]:	dissolution rate normalized to BET surface area
$Rate_H$ [mol m^{-2} h^{-1}]:	proton-promoted dissolution rate (Eqn. 28)
$Rate_{SS1}$ [mol m^{-2} h^{-1}]:	steady state dissolution rate at pH 1 normalized to BET surface area; equal to $k_{SS1}[>M_{SS1}]$
t [h]:	time
τ [h]:	time constant defining the rate of accumulation of the metal of interest within a CSTR in response to a step function change in input concentration (e.g., a change in inlet concentration or mineral dissolution rate) from one constant rate of input to a new constant rate of input; equal to the mean residence time of solution within the reactor, $V q^{-1}$
τ_{NSS} [h]:	time constant defining the rate of accumulation of the metal of interest within a CSTR in response to an increase in mineral dissolution rate from zero to a nonsteady state rate; equal to $V/(q-Vk_1)$; subscripts denote τ for specific site types
τ_{EX} [h]:	total excess dissolution-active sites; $V/(q-Vk_{EX})$
τ_{EXF} [h]:	fast-dissolving excess sites; $V/(q-Vk_{EXF})$
τ_{EXS} [h]:	slow-dissolving excess sites; $V/(q-Vk_{EXS})$
τ_{PI} [h]:	excess sites whose dissolution is perceived as a pulse input; $V/(q-Vk_{PI})$
V [L]:	reactor volume